

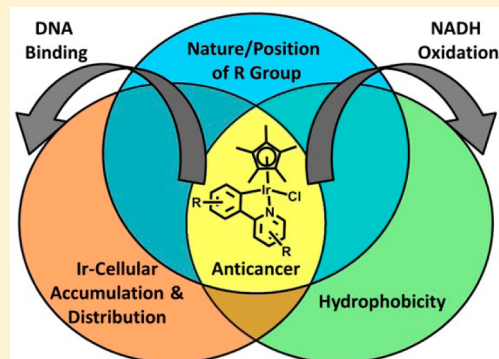
Contrasting Anticancer Activity of Half-Sandwich Iridium(III) Complexes Bearing Functionally Diverse 2-Phenylpyridine Ligands

Adam J. Millett, Abraha Habtemariam, Isolda Romero-Canelón, Guy J. Clarkson, and Peter J. Sadler*

Department of Chemistry, University of Warwick, Gibbet Hill Road, Coventry, CV4 7AL, U.K.

S Supporting Information

ABSTRACT: We report the synthesis, characterization, and antiproliferative activity of 15 iridium(III) half-sandwich complexes of the type $[(\eta^5\text{-Cp}^*)\text{Ir}(2\text{-}(R'\text{-phenyl})\text{-R-pyridine})\text{Cl}]$ bearing either an electron-donating ($-\text{OH}$, $-\text{CH}_2\text{OH}$, $-\text{CH}_3$) or electron-withdrawing ($-\text{F}$, $-\text{CHO}$, $-\text{NO}_2$) group at various positions on the 2-phenylpyridine (2-PhPy) chelating ligand giving rise to six sets of structural isomers. The X-ray crystal structures of $[(\eta^5\text{-Cp}^*)\text{Ir}(2\text{-}(2'\text{-fluorophenyl})\text{pyridine})\text{Cl}]$ (1) and $[(\eta^5\text{-Cp}^*)\text{Ir}(2\text{-}(4'\text{-fluorophenyl})\text{pyridine})\text{Cl}]$ (2) exhibit the expected “piano-stool” configuration. DFT calculations showed that substituents caused only localized effects on the electrostatic potential surface of the chelating 2-PhPy ligand of the complexes. Hydrolysis of all complexes is rapid, but readily reversed by addition of NaCl. The complexes show preferential binding to 9-ethylguanine over 9-methyladenine and are active catalysts for the oxidation of NADH to NAD^+ . Antiproliferative activity experiments in A2780 ovarian, MCF-7 breast, A549 lung, and HCT116 colon cancer cell lines showed IC_{50} values ranging from 1 to $89 \mu\text{M}$, with the most potent complex, $[(\eta^5\text{-Cp}^*)\text{Ir}(2\text{-}(2'\text{-methylphenyl})\text{pyridine})\text{Cl}]$ (13) ($\text{A2780 } \text{IC}_{50} = 1.18 \mu\text{M}$), being 10 \times more active than the parent, $[(\eta^5\text{-Cp}^*)\text{Ir}(2\text{-phenylpyridine})\text{Cl}]$, and 2 \times more active than $[(\eta^5\text{-Cp}^{\text{xPh}})\text{Ir}(2\text{-phenylpyridine})\text{Cl}]$. Intriguingly, contrasting biological activities are observed between structural isomers despite exhibiting similar chemical reactivity. For pairs of structural isomers both the nature and position of the functional group can affect the hydrophobicity of the complex. An increase in hydrophobicity resulted in enhanced cellular-iridium accumulation in A2780 ovarian cells, which generally gave rise to an increase in potency. The structural isomers $[(\eta^5\text{-Cp}^*)\text{Ir}(2\text{-}(4'\text{-fluorophenyl})\text{pyridine})\text{Cl}]$ (2) and $[(\eta^5\text{-Cp}^*)\text{Ir}(2\text{-phenyl-5-fluoropyridine})\text{Cl}]$ (4) preferentially localized in the cytosol > membrane and particulate > nucleus > cytoskeleton. This work highlights the strong dependence of biological behavior on the nature and position of the substituent on the chelating ligand and shows how this class of organometallic anticancer complexes can be fine-tuned to increase their potency without using extended cyclopentadienyl systems.



INTRODUCTION

There is an increasing interest in the design of organometallic anticancer complexes,¹ especially complexes that are active against cisplatin-resistant cancers,² and organo-iridium(III) complexes are showing promise in this regard.³ We have reported that the biological activity of half-sandwich penta-methylcyclopentadienyl (Cp^*) iridium(III) complexes can be increased by the incorporation of phenyl substituents, as in Cp^{xPh} and Cp^{xBiPh} ligands.⁴ This increase in activity may be due in part to an increase in hydrophobicity, resulting in enhanced cellular accumulation. Extended cyclopentadienyl systems have also been shown to strengthen interactions with DNA via intercalation between DNA base pairs.^{4a} The introduction of the negatively charged C,N -chelating ligands in place of neutral N,N ligands has also been shown to improve antiproliferative activity.⁵ Again, the increase in activity may be attributed to an increase in hydrophobicity of the resulting neutral complex. Anionic ligands in place of neutral ligands in other iridium systems have also been explored.^{3e,6}

Chelated half-sandwich iridium(III) complexes have been shown to bind to DNA nucleobases via the monodentate site and can inhibit the synthesis of DNA by DNA polymerases.^{4a} Some of these complexes also inhibit thioredoxin reductase 1 (Trx-R).⁷ Intriguingly they can also catalyze the oxidation of NADH to NAD^+ , and modulation of the NAD^+/NADH ratio has been demonstrated in A2780 human ovarian cancer cells.⁸ Disruption of this redox process may contribute to a multitargeting mechanism of action.⁹ Recently we reported that the highly potent and selective C,N -chelated complex $[(\eta^5\text{-C}_6\text{H}_3\text{C}_6\text{H}_4\text{Cp}^*)\text{Ir}(2\text{-PhPy})\text{pyridine}]\text{PF}_6$, which bears pyridine in place of chloride as a monodentate ligand, can produce H_2O_2 upon the catalytic reaction with NADH via hydride transfer to molecular O_2 .¹⁰

The effect of incorporating functionality on the chelating ligand in half-sandwich iridium(III) anticancer complexes has

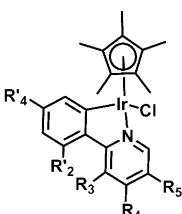
Special Issue: Mike Lappert Memorial Issue

Received: February 3, 2015

Published: March 25, 2015

not been widely explored.^{7,11} The aim of the present research was to synthesize a novel set of complexes bearing functionally diverse 2-PhPy ligands. 2-PhPy has shown promise in half-sandwich iridium anticancer complexes.^{5,12} Synthesis of 15 2-PhPy ligands that bear either -F, -CHO, -NO₂, -OH, -CH₂OH, or -CH₃ functional groups on different positions on the chelating ligand (Chart 1) was accomplished by

Chart 1. $[(\eta^5\text{-Cp}^*)\text{Ir}(2\text{-(R}'\text{-phenyl)-R-pyridine})\text{Cl}]$ Complexes Studied in This Work



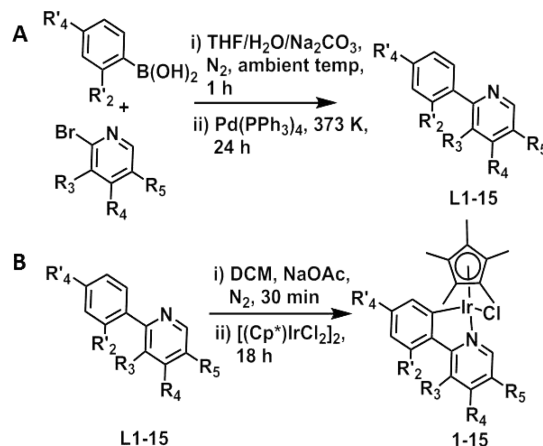
Complex	R ₄	R ₂	R ₃	R ₄	R ₅
1	H	F	H	H	H
2	F	H	H	H	H
3	H	H	F	H	H
4	H	H	H	H	F
5	CHO	H	H	H	H
6	H	H	H	H	CHO
7	NO ₂	H	H	H	H
8	H	H	H	NO ₂	H
9	CH ₂ OH	H	H	H	H
10	H	H	H	CH ₂ OH	H
11	OH	H	H	H	H
12	H	H	H	H	OH
13	H	CH ₃	H	H	H
14	H	H	H	CH ₃	H
15	H	H	H	H	CH ₃

employing Suzuki–Miyaura palladium cross-coupling. The resulting 15 novel iridium(III) Cp* complexes $[(\eta^5\text{-Cp}^*)\text{Ir}(2\text{-(R}'\text{-phenyl)-R-pyridine})\text{Cl}]$ (Chart 1) have been investigated for their aqueous chemistry, electrostatic potential surfaces (EPS), interaction with model DNA nucleobases, and ability to catalyze the oxidation of reduced coenzyme nicotine adenine dinucleotide NADH to NAD⁺. Correlations between relative hydrophobicity, cellular accumulation of iridium, and anti-proliferative activity have been studied, along with comparisons of the cellular distributions of a pair of structural isomers. Importantly it is apparent that within this series there are potent complexes even without the presence of extended cyclopentadienyl systems.

RESULTS

Synthesis and Characterization of $[(\eta^5\text{-Cp}^*)\text{Ir}(2\text{-(R}'\text{-phenyl)-R-pyridine})\text{Cl}]$ Complexes. Suzuki–Miyaura cross-coupling chemistry was employed following an adapted protocol,¹³ to synthesize chelating 2-PhPy ligands with electron-donating or electron-withdrawing substituents, Scheme 1. They were purified using flash silica gel chromatography with mixtures of chloroform/ethyl acetate, yielding 2-(R'-phenyl)-R-pyridine ligands L1–15. The synthesis of the corresponding complexes $[(\eta^5\text{-Cp}^*)\text{Ir}(2\text{-(R}'\text{-phenyl)-R-pyridine})\text{Cl}]$ (1–15) was carried out using an adapted literature procedure.^{4b} The synthetic routes for the complexes are shown in Scheme 1. The introduction of electron-withdrawing nitro (-NO₂) and aldehydic (-CHO) groups and an electron-donating hydroxymethyl group (-CH₂OH) in complexes 5–10 is the first to be reported in

Scheme 1. Synthetic Route for 2-(R'-phenyl)-R-pyridine Ligands L1–15 (A) and $[(\eta^5\text{-Cp}^*)\text{Ir}(2\text{-(R}'\text{-phenyl)-R-pyridine})\text{Cl}]$ Complexes 1–15 (B)



complexes of the type $[(\eta^5\text{-Cp}^*)\text{Ir}(2\text{-PhPy})\text{X}]^{0/+}$. The complexes were characterized by ¹H and ¹³C NMR spectroscopy, ESI-MS, CHN analysis, and RP-HPLC. Crystals of complexes 1 and 2 suitable for structure determination by X-ray diffraction were obtained by slow evaporation from chloroform/hexane at 273 K.

Molecular Structures. The X-ray crystal structures of complexes $[(\eta^5\text{-Cp}^*)\text{Ir}(2\text{-(2'-fluorophenyl)pyridine})\text{Cl}]$ (1) and $[(\eta^5\text{-Cp}^*)\text{Ir}(2\text{-(4'-fluorophenyl)pyridine})\text{Cl}]$ (2) were determined by X-ray diffraction and are shown in Figure 1.

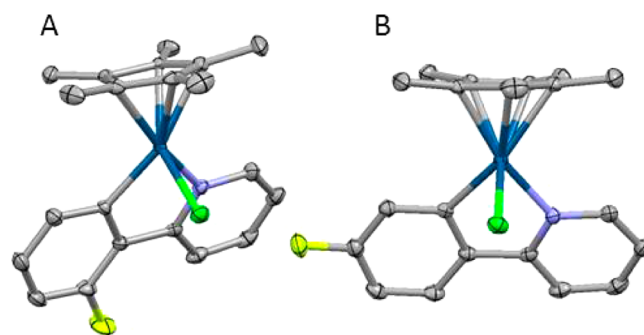


Figure 1. X-ray crystal structures of compounds 1 (A) and 2 (B). Hydrogen atoms have been omitted for clarity, and thermal ellipsoids are shown at 50% probability. The disorder observed for complex 1 has been removed for clarity, but is described in the Supporting Information.

X-ray crystallographic data are listed in Table S1, and selected bond lengths and angles in Table 1. The complexes exhibit the expected pseudo-octahedral half-sandwich structure, with the Cp* ring occupying three coordination sites, the 2-PhPy chelating ligand occupying two sites, and the monodentate chlorido ligand occupying the sixth coordination position. Ir–centroid distances are 1.828 and 1.833 Å for 1 and 2, respectively, while the Ir–C distances of 2.0482(18) and 2.0346(19) Å and Ir–N distances of 2.0797(17) and 2.0931(16) Å show significant variation and Ir–Cl distances of 2.4056(5) and 2.4026(5) Å show small ($>3\sigma$) differences for complexes 1 and 2, respectively. The bond angles are similar, with the angle between the chelating ligand and iridium center (C–Ir–N) being the smallest, 77.84(7)° and 78.13(7)° for 1 and 2, respectively. Weak offset intermolecular π – π stacking

Table 1. Selected Bond Lengths (Å) and Bond Angles (deg) for Complexes 1 and 2

bond/angle	1	2
Ir–C (Cp* ring)	2.163(2)	2.160(2)
	2.1675(19)	2.1609(19)
	2.177(2)	2.172(2)
	2.239(2)	2.2522(19)
	2.247(2)	2.272(2)
Ir–C (centroid)	1.828	1.833
	2.0482(18)	2.0346(19)
Ir–N	2.0797(17)	2.0931(16)
Ir–Cl	2.4056(5)	2.4026(5)
C–Ir–N	77.84(7)	78.13(7)
C–Ir–Cl	85.96(5)	85.68(5)
N–Ir–Cl	87.60(5)	87.30(5)

between the 2-PhPy ligands is observed for both complexes with a centroid–centroid distance of 4.140 Å in complex 1 and 4.059 Å in complex 2 (Figure S1).

Electrostatic Potential Surface. The EPSs of complexes 2, 4, 7, 8, and 11–13 were calculated using DFT methods at the PBE0/LanL2DZ/6-31+G** level,¹⁴ based on the crystal structure of complex 2, with functional group modifications being made with GaussView 3.0.¹⁵ The resulting EPS of each complex is shown in Figure 2. The phenyl ring in the chelating ligand exhibits a more negative electrostatic potential than the pyridyl ring due to the deprotonated carbon bound to the Ir center. There are no major differences in the charge distribution at the iridium center, Cp* ring, or chlorido ligands among the complexes, indicating that the substituent on the chelating ligand causes only a localized effect. Complexes 7 and 8 contain the electron-withdrawing nitro group on the phenyl and pyridyl ring, respectively, causing a more positive surface. Complex 13 bears a methyl group on the phenyl ring, which pushes electron density into the ring, causing a more negative EPS. The substituents themselves cause the outer EPS of each complex to alter significantly. The calculated bond lengths at the metal center are shown in Table S2, which shows minimal differences among the complexes, with the exception of 13, which exhibits a shorter Ir–N bond. The HOMO and LUMO orbitals of complexes 2, 4, 7, 8, and 11–13 and corresponding orbital energies are shown in Table S3.

Hydrolysis Studies. The hydrolysis of complexes 1–15 (ca. 500 μM) was studied by ¹H NMR spectroscopy in 26.7% MeOD-*d*₄/73.3% D₂O at 310 K. Methanol was required to ensure the solubility of the complexes in aqueous solution. Hydrolysis equilibrium was reached before the time taken to acquire the first spectra (15 min), consistent with previous reports of Ir^{III} C,N-chelated half-sandwich complexes.^{4b} Between 67% and 80% was found to be in the hydrolyzed form, based on peak integrations. Hydrolysis was confirmed by the sequential addition of NaCl, showing an increase in the peaks associated with the Ir–Cl species and a decrease in the peaks associated with the Ir–OD₂/OD species. With 4 mM NaCl present, almost all of the Ir–OD₂/OD species had been converted to the Ir–Cl complexes (Figure S2). Above this concentration of NaCl, precipitation of the complexes was observed.

Binding to Nucleobases. Complexes 2, 4, 7, 8, and 11–14 (ca. 500 μM) were evaluated for their ability to bind to 9-ethylguanine (9-EtG) and 9-methyladenine (9-MeA) in ca. 1:1

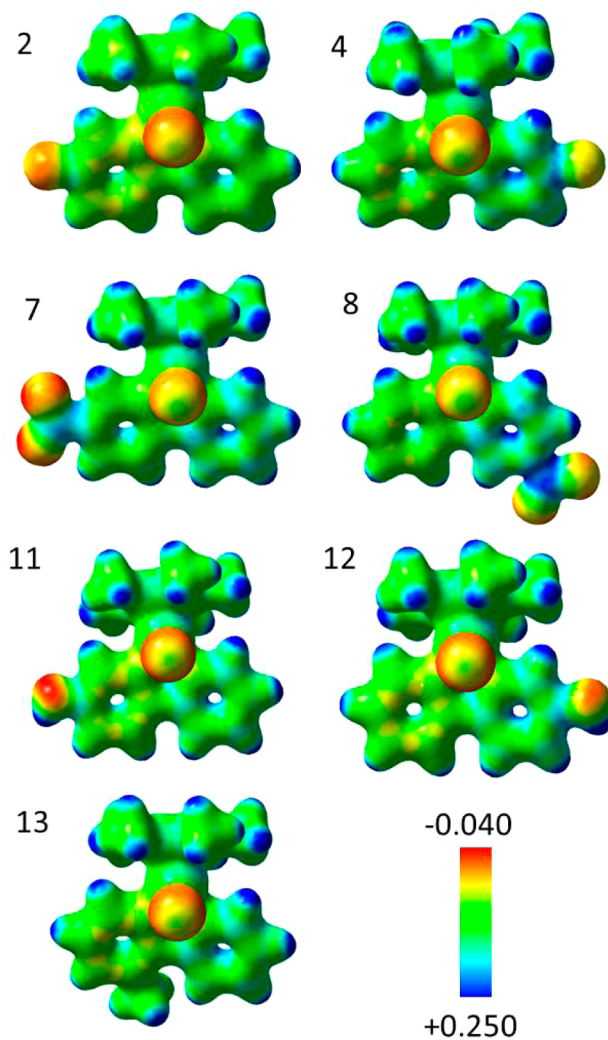


Figure 2. Electrostatic potential surfaces for complexes 2, 4, 7, 8, and 11–13 (calculated at the PBE0/LanL2DZ/6-31+G** level), where the EPSs are shown both in space (with positive and negative regions in blue and red, respectively) and mapped on electron density (isovalue 0.04) of the molecules. The electrostatic potential is represented with a color scale ranging from red (–0.040 au) to blue (+0.250 au). Note the more negative charge distribution on the phenyl ring of the 2-PhPy chelating ligand compared with the pyridyl ring. The substituents affect markedly only the electronic charge density on the chelating ligand, leaving the iridium center, Cp*, and chlorido ligands relatively unaffected.

mol ratios of complex to nucleobase by ¹H NMR spectroscopy in 26.7% MeOD-*d*₄/73.3% D₂O at 310 K, pH* 7.4, after incubation for 15 min and 24 h. All complexes showed 100% binding to 9-EtG and ca. 50–80% binding to 9-MeA after 15 min, which remained unchanged over a period of 24 h. Competitive binding studies between 9-EtG and 9-MeA were also performed under the same conditions. This resulted in mostly 9-EtG binding for all the complexes (Figure 3). Complexes 2, 4, and 14 show 5–10% binding to 9-MeA in the presence of 9-EtG. Binding of 9-EtG to 2 and 4 in the presence of 4 mM NaCl, where the complexes exist primarily as the Ir–Cl species, reached 100% after 24 h (Figure S3).

Catalysis of NADH Oxidation. The reaction between NADH and complexes 2, 4, 11, and 12 was monitored by UV–vis spectroscopy at varying concentrations of NADH (69, 103, and 146 μM) with a fixed concentration of complex (2.5 μM)

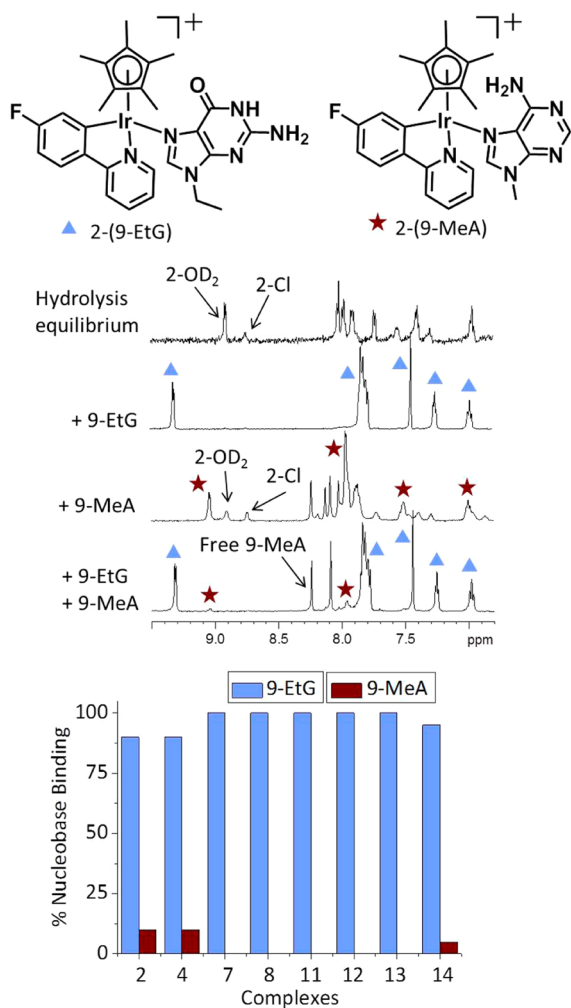


Figure 3. (Top) Interaction of complex **2** (ca. 500 μM) with equimolar amounts of 9-EtG and 9-MeA and competition binding by ^1H NMR spectroscopy (600 MHz, 26.7% MeOD- d_4 /73.3% D_2O at 310 K, $\text{pH}^* 7.4$, 24 h). Complex **2** shows 100% binding to 9-EtG (blue triangles) and around 50% binding to 9-MeA (red stars). Complex **2** shows a preference for binding to 9-EtG upon co-incubation with 9-EtG and 9-MeA. (Bottom) Co-incubation of complexes **2**, **4**, **7**, **8**, and **11–14** with equimolar amounts of 9-EtG and 9-MeA showing a preference for binding to 9-EtG.

over a period of 24 h at 310 K, $\text{pH} 7.5$ ($\text{Na}_2\text{HPO}_4/\text{NaH}_2\text{PO}_4$ buffer, 5 mM). The decrease in the band at 339 nm was monitored, as it corresponds to conversion of NADH to NAD^+ (Figure 4a). The data were also the basis for the calculation of the turnover number (TON) and turnover frequency (TOF, h^{-1}) for each complex at different concentrations (Table 2). After 24 h, the maximum TON was found for each complex at the highest concentration of NADH (146 μM) and ranged from 22 to 28. Maximum TOF was also reached at 146 μM NADH, ranging from 1.1 to 3.2 h^{-1} . The reaction proceeded via first-order kinetics with respect to $[\text{NADH}]$ (Figure 4b), with an average rate constant k of $3.79 \times 10^{-4} \text{ min}^{-1}$ for **2** and $4.03 \times 10^{-4} \text{ min}^{-1}$ for **4**. However, complexes **11** and **12**, which bear the hydroxyl group, gave a non-first-order reaction with respect to $[\text{NADH}]$ during the first 3 h, followed by the expected first-order kinetics (exemplified for complex **11** in Figure S4). These results indicate that each of these complexes shows catalytic behavior toward the oxidation of NADH.

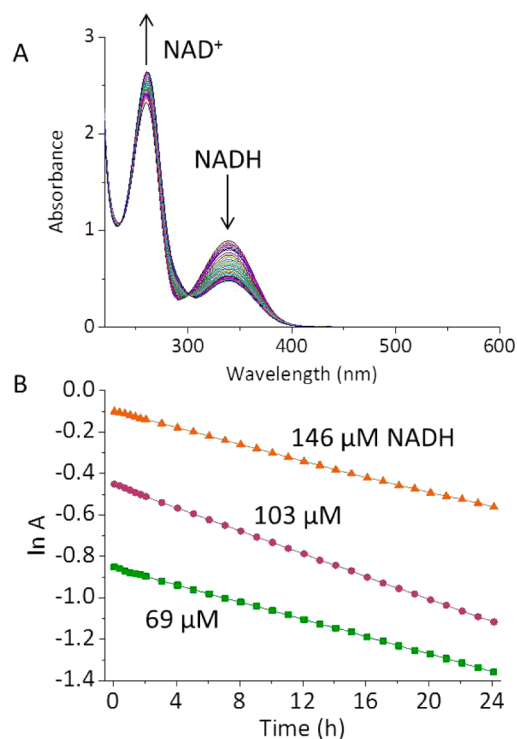


Figure 4. (a) UV–visible spectra for the catalytic oxidation of NADH (146 μM) to NAD^+ in the presence of complex **2** (2.5 μM) over a 24 h period in 0.5% MeOH/99.5% H_2O at 310 K in 5 mM $\text{Na}_2\text{HPO}_4/\text{NaH}_2\text{PO}_4$ buffer, $\text{pH} 7.5$. (b) First-order kinetic plot. $[\text{NADH}] = 69 \mu\text{M}$ (green), 103 μM (purple), and 146 μM (orange).

In order to probe whether the oxidation proceeds via the formation of an iridium-hydride species, the reaction of complex **2** (250 μM) with NADH (750 μM) in 50% MeOD- d_4 /50% D_2O at 310 K was monitored by ^1H NMR spectroscopy over a 15 h period. After 15 min, a peak corresponding to an Ir–H species was observed at -14.84 ppm (Figure S5), which was no longer visible after 15 h. The conversion of NADH to NAD^+ was also confirmed by the appearance of a new set of peaks corresponding to the formation of NAD^+ .

Antiproliferative Activity. The antiproliferative activity of complexes **1–15** in A2780 (ovarian) cancer cells and complexes **1, 2, 5, 6, 8, 10, 11, and 14** in HCT-116 (colon), MCF-7 (breast), and A549 (lung) cancer cells is shown in Table 3. The activity of previously reported^{4b} iridium complexes $[(\eta^5\text{-Cp}^*)\text{Ir}(2\text{-phenylpyridine})\text{Cl}]$ (**16**) and $[(\eta^5\text{-Cp}^{\text{ph}})\text{Ir}(2\text{-phenylpyridine})\text{Cl}]$ (**17**) with no substituents on the chelating ligand is also shown for comparison. It is evident that the presence of substituents on the chelating ligand greatly affects the antiproliferative activity of the complexes, with IC_{50} values ranging from 1 to 60 μM in the A2780 cell line alone. $[(\eta^5\text{-Cp}^*)\text{Ir}(2\text{-}(2'\text{-methylphenyl})\text{pyridine})\text{Cl}]$ (**13**) is the most potent complex, with an IC_{50} value of 1.18 μM in A2780 ovarian cancer cells, making it more potent than the extended cyclopentadienyl complex $[(\eta^5\text{-Cp}^{\text{ph}})\text{Ir}(2\text{-phenylpyridine})\text{Cl}]$. Complexes **2, 8, 13, and 15** also show similar potency to the clinical drug cisplatin (CDDP). Interestingly, structural isomers exhibit contrasting activities, for example, complexes $[(\eta^5\text{-Cp}^*)\text{Ir}(2\text{-}(4'\text{-fluorophenyl})\text{pyridine})\text{Cl}]$ (**2**) (2.7 μM) and $[(\eta^5\text{-Cp}^*)\text{Ir}(2\text{-phenyl-5-fluoropyridine})\text{Cl}]$ (**4**) (>60 μM) and complexes $[(\eta^5\text{-Cp}^*)\text{Ir}(2\text{-}(4'\text{-hydroxyphenyl})\text{pyridine})\text{Cl}]$

Table 2. Calculated TONs and TOFs for Complexes **2**, **4**, **11**, and **12** for the Catalytic Oxidation of NADH to NAD⁺ Monitored via UV–Visible Spectroscopy at Various Concentrations of NADH (69, 103, and 146 μM) with a Fixed Complex Concentration of 2.5 μM over a 24 h Period in 0.5% MeOH/99.5% H₂O at 310 K in 5 mM Na₂HPO₄/NaH₂PO₄ Buffer, pH 7.5^a

complex	NADH conc (μM)	TON (24 h)	TOF (h^{-1}) ^b
[(η^5 -Cp*)Ir(2-(4'-fluorophenyl)pyridine)Cl], 2	69	11	0.6
	103	19	1.1
	146	22	1.2
[(η^5 -Cp*)Ir(2-phenyl-5-fluoropyridine)Cl], 4	69	13	0.7
	103	20	1.2
	146	22	1.1
[(η^5 -Cp*)Ir(2-(4'-hydroxyphenyl)pyridine)Cl], 11	69	14	1.9
	103	21	2.6
	146	28	3.2
[(η^5 -Cp*)Ir(2-phenyl-5-hydroxypyridine)Cl], 12	69	13	1.4
	103	15	1.8
	146	22	2.6

^aThe conversion of NADH to NAD⁺ was followed from the absorption at 339 nm. ^bTOFs were calculated as the gradient of time vs TON during the first 2 h of the reaction time.

Table 3. IC₅₀ Values for Complexes **1–15** in A2780 Cells and Complexes **1**, **2**, **5**, **6**, **8**, **10**, **11**, and **14** in HCT-116, MCF-7, and A549 Cells^a

complex	IC ₅₀ values (μM)			
	A2780	HCT-116	MCF-7	A549
1	4.5 \pm 0.2	3.7 \pm 0.3	9.6 \pm 0.4	10.36 \pm 0.07
2	2.7 \pm 0.3	6.8 \pm 0.1	4.8 \pm 0.3	2.1 \pm 0.3
3	>50	n.d.	n.d.	n.d.
4	>60	n.d.	n.d.	n.d.
5	6.9 \pm 0.3	21.3 \pm 0.7	11.6 \pm 0.5	15.8 \pm 0.4
6	4.4 \pm 0.4	18.8 \pm 0.5	6.5 \pm 0.3	5.9 \pm 0.1
7	24.73 \pm 2.30	n.d.	n.d.	n.d.
8	2.7 \pm 0.1	27.5 \pm 0.9	11.4 \pm 0.4	20.1 \pm 0.3
9	>50	n.d.	n.d.	n.d.
10	47 \pm 1	57.3 \pm 0.9	47 \pm 2	89 \pm 1
11	47.3 \pm 0.1	29.3 \pm 0.8	28.6 \pm 0.9	56.67 \pm 0.04
12	13.29 \pm 0.88	n.d.	n.d.	n.d.
13	1.18 \pm 0.08	n.d.	n.d.	n.d.
14	3.9 \pm 0.2	9.6 \pm 0.6	3.7 \pm 0.1	8.7 \pm 0.3
15	1.26 \pm 0.01	n.d.	n.d.	n.d.
16^b	10.78 \pm 1.72	n.d.	n.d.	n.d.
17^b	2.14 \pm 0.50	n.d.	n.d.	n.d.
cisplatin	1.2 \pm 0.2	5.2 \pm 0.3	7.0 \pm 0.1	3.5 \pm 0.2

^aDrug exposure time was 24 h followed by a 72 h recovery time. All values were determined as independent duplicates of triplicate experiments, and the standard deviations were calculated. ^bFrom ref 4b.

(**11**) (47.3 μM) and [(η^5 -Cp*)Ir(2-phenyl-5-hydroxypyridine)Cl] (**12**) (13.29 μM).

Relative Hydrophobicity. The relative hydrophobicities of complexes **2/4**, **7/8**, **11/12**, and **13/14** (four pairs of structural isomers) were determined by RP-HPLC. The more hydrophobic complexes have longer retention times (t_R). To ensure solubility of the complexes, methanol was used (MeOH/H₂O, 1:9 v/v) with NaCl (50 mM) to suppress the hydrolysis of the complexes in both sample preparation and in the HPLC solvents. The resulting retention times are shown in Table 4. Complex **11** shows the shortest retention time (least hydrophobic) at 15.11 min, while complex **14** shows the longest retention time (most hydrophobic) at 20.9 min.

Table 4. Retention Times (t_R) by RP-HPLC and Cellular-Iridium Accumulation (at Equipotent (IC₅₀) Concentrations) in A2780 Cells for Complexes **2**, **4**, **7**, **8**, and **11–14**

complex	2-PhPy ligand	t_R (min)	cellular-Ir (ng Ir \times 10 ⁶ A2780 cells)
2	2-(4'-fluorophenyl)pyridine	18.74 \pm 0.05	13.5 \pm 0.3
4	2-phenyl-5-fluoropyridine	18.60 \pm 0.02	11.1 \pm 0.1
7	2-(4'-nitrophenyl)pyridine	18.8 \pm 0.2	8 \pm 1
8	2-phenyl-4-nitropyridine	18.0 \pm 0.1	9.0 \pm 0.2
11	2-(4'-hydroxyphenyl)pyridine	15.11 \pm 0.03	1.6 \pm 0.1
12	2-phenyl-5-hydroxypyridine	17.8 \pm 0.2	10.2 \pm 0.2
13	2-(2'-methylphenyl)pyridine	20.4 \pm 0.2	18 \pm 1
14	2-phenyl-5-methylpyridine	20.9 \pm 0.9	16.0 \pm 0.3

Cellular-Iridium Accumulation. Cellular-iridium accumulation in A2780 cells after 24 h exposure to complexes **2**, **4**, **7**, **8**, and **11–14** at equipotent (IC₅₀) concentrations was determined by ICP-MS and is shown in Table 4. Complex **11** shows the lowest accumulation of 1.58 ng Ir \times 10⁶ cells, while complex **13** exhibits the highest extent of accumulation of 18.46 ng Ir \times 10⁶ cells.

Cellular-Iridium Distribution. Structural isomers **2** and **4** were examined for their cellular-iridium distribution in A2780 human ovarian cancer cells at IC₅₀ concentrations, Figure 5. The cytosol contains the highest amount of iridium (51.4% for **2** and 69.2% for **4**), followed by the cell membrane and particulate fractions (28.4% for **2** and 17.9% for **4**). Complex **4** localizes in the cytosol to a greater extent than complex **2** ($p < 0.01$), which in turn localizes in the cell membrane to a greater extent than **4** ($p < 0.01$). The nuclear fraction contains different amounts of iridium, with 10.4% and 6.7% ($p < 0.01$) for complexes **2** and **4**, respectively, while the cytoskeletal fraction contains similar levels of iridium, with 9.8% and 6.1% ($p > 0.05$) for **2** and **4**, respectively.

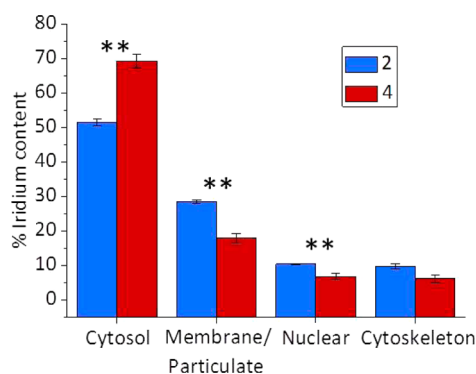


Figure 5. Cellular-iridium distribution of structural isomers **2** and **4** in A2780 human ovarian cancer cells. Complex **4** localizes in the cytosol to a greater extent than **2**, while complex **2** localizes in the membrane and particulate fractions to a greater extent than **4**. Student's *t* test at *p* < 0.01 level indicated by **.

DISCUSSION

Synthesis and Characterization. The synthesis of complexes **1–15** was carried out using an adapted literature procedure.^{4b} It was found that the reported reaction time of 2 h was not sufficient to provide **1–15** in good yields; therefore it was extended to 18 h to obtain yields ranging from 16% to 80%. Low yields were obtained for complexes **9** and **12** (22% and 16%, respectively) due to their poor solubility in chlorinated solvents, preventing efficient separation of the complexes from sodium acetate used to deprotonate the carbon on the phenyl ring. The characterization of complexes **1–15** was done by ¹H NMR, ESI-MS, CHN analysis, HPLC, and in most cases ¹³C NMR. The ¹H NMR spectra are characterized by one less proton in the low-field region compared to the starting 2-PhPy ligand, due to the deprotonation of the bound carbon on the phenyl ring. No appreciable difference in the ¹H NMR chemical shift of the Cp* ligand was observed among the functionally diverse complexes. The ¹³C NMR spectra of fluorine-containing complexes **1**, **3**, and **4** show coupling to ¹⁹F with ¹J_{CF} = 249–258 Hz, values similar to those previously reported.¹⁶ The ESI-MS of the complexes always showed an *m/z* peak corresponding to $\{(\eta^5\text{-Cp}^*)\text{Ir}(2\text{-}(\text{R}'\text{-phenyl})\text{-R-pyridine})\}^+$, where the chlorido ligand had been removed in the ionization process to form a detectable positive-ion peak. RP-HPLC was also utilized to determine the purity of the complexes, and examples of chromatograms are shown in the Supporting Information (Figure S7).

Complexes $[(\eta^5\text{-Cp}^*)\text{Ir}(2\text{-}(2'\text{-fluorophenyl})\text{pyridine})\text{Cl}]$ (**1**) and $[(\eta^5\text{-Cp}^*)\text{Ir}(2\text{-}(4'\text{-fluorophenyl})\text{pyridine})\text{Cl}]$ (**2**) exhibit the “piano-stool” structure expected for half-sandwich metal complexes with bond lengths/angles comparable to similar previously reported structures.^{4b,17} However, the position of the fluorine on the phenyl ring influences the Ir-chelating ligand bond lengths. Complex **2** exhibits a shorter Ir–C bond and a longer Ir–N bond length than **1**, suggesting that the binding affinity of N and C for the Ir center is different. Therefore, changing the position at which electron density is withdrawn affects the solid-state structure of the complex. Both complexes exhibit weak offset π – π stacking between the 2-PhPy ligand, with a centroid–centroid distance of 4.140 Å for **1** and 4.059 Å for **2**.

DFT calculations on complexes **2**, **4**, **7**, **8**, and **11–13** indicate that the presence of substituents does not affect the electronic density on the iridium center, Cp* ring, or chlorido

ligands, which implies that the reactivity at the metal center may remain relatively the same for all complexes. The EPS also shows that the phenyl ring in the chelating ligand has a more negative electrostatic potential than the pyridyl ring, due to the negative charge associated with the deprotonation of the binding carbon. The electron-withdrawing/electron-donating nature of the substituents affects the EPS of the chelating ligand by either diminishing or enhancing the electronic charge density on the ring system to which the substituent is bound. The electron-withdrawing –NO₂ and –F groups provide a more positive EPS within the ring, while the electron-donating –OH and –CH₃ groups generate a more negative EPS within the ring. The presence of the substituents significantly changes the EPS of the chelating ligand, with areas of higher electronic charge density for complexes **2**, **4**, **7**, **8**, **11**, and **12** due to the presence of heteroatoms with differing electronegativities. As weak electrostatic forces are often important for binding and recognition interactions with biomolecules such as peptides, proteins, and enzymes,¹⁸ the nature and position of the substituent may play a significant role in the interaction of the complexes studied here with target sites.

Aqueous Chemistry. Hydrolysis studies by ¹H NMR showed that all complexes are converted to an equilibrium mixture of Ir–Cl and Ir–OD₂/OD at 310 K within the time taken to complete the first spectrum (15 min) with 67–80% existing as the aqua/hydroxido adduct. This is consistent with previous findings that iridium(III) half-sandwich complexes can exhibit fast rates of ligand exchange^{4a,19} in comparison to their non-“piano stool” octahedral counterparts.²⁰ Previous reports on the aqua adducts of C,N-chelated half-sandwich iridium(III) complexes showed that the pK_a values are in the range 8.3–8.9;^{4b} therefore the complexes studied here are likely to exist as the aqua rather than the hydroxido adduct at physiological pH. The presence of substituents on the 2-PhPy chelating ligand does not appear to affect the rate or extent of hydrolysis. The hydrolysis can be readily reversed by addition of NaCl, and a concentration of 4 mM NaCl almost completely suppresses hydrolysis. This would imply that at biologically relevant chloride concentrations (i.e., in the nucleus) the complexes would exist as the Ir–Cl rather than aqua species.

Interactions with Nucleobases. DNA is a major target for many transition metal anticancer compounds.²¹ The interaction of complexes **2**, **4**, **7**, **8**, and **11–14** with DNA nucleobases 9-EtG and 9-MeA indicated a strong preference for 9-EtG, with 100% binding after 15 min. Complexes **2** and **4** also exhibited 100% binding to 9-EtG after 15 min even in the presence of 4 mM NaCl, where the complex exists as the Ir–Cl species. All complexes were able to bind to 9-MeA, but only complexes **2**, **4**, and **14** formed any significant amount of 9-MeA adducts in competition binding experiments with 9-EtG, highlighting that binding to 9-MeA was less strong than to 9-EtG. The weaker binding of 9-MeA may be attributed to the steric hindrance caused by the –NH₂ group at the 4 position. Guanine is also known to be a better electron donor than adenine, which may also contribute to the selectivity in 9-EtG binding.²² Guanine is therefore a potential binding site on DNA, as it is for cisplatin,^{21a} and other transition metal anticancer complexes.²³

Catalysis of NADH Oxidation. The potential for complexes **2**, **4**, **11**, and **12** to catalytically modulate the NAD⁺/NADH ratio in cells was examined. All exhibited catalytic activity toward the conversion of NADH to NAD⁺ by first-order reaction kinetics with respect to [NADH]. Complex **11** exhibits the best catalytic activity, with a TON of 28 and

TOF of 3.2 h^{-1} ($[\text{NADH}] = 146 \mu\text{M}$), while **2** and **4** have the lowest TON of 22 and TOF of 1.2 and 1.1 h^{-1} , respectively. The presence of the hydroxyl group in **11** and **12** seems to enhance the catalytic activity. Complexes **11** and **12** also exhibited an unusual kinetic profile for the first 3 h of reaction time, followed by the expected first-order kinetics. The hydroxyl group on complex $[(\eta^5\text{-Cp}^*)\text{Ir}(2\text{-phenyl-6-hydroxypyridine})\text{Cl}]$ has been previously reported to be integral to the catalytic activity toward the dehydrogenative oxidation of organic compounds,²⁴ which implies that the hydroxyl group may be involved in the catalytic cycle. Although the position of the hydroxyl group in **11** and **12** is situated further from the metal center than in $[(\eta^5\text{-Cp}^*)\text{Ir}(2\text{-phenyl-6-hydroxypyridine})\text{Cl}]$, the unusual kinetics observed may indicate that it is initially playing a role in the catalytic activity. It has been suggested that the rate-limiting step in this catalytic reaction is the formation of the Ir-NADH adduct, leading to first-order reaction kinetics with respect to $[\text{NADH}]$;^{8b} therefore the unusual kinetic profile of **11** and **12** may involve participation of the hydroxyl group on the chelating ligand. The involvement of the ligand in the oxidation of NADH in half-sandwich iridium(III) complexes has not been previously observed. The oxidation of NADH proceeds via formation of an Ir-H species as observed in the ^1H NMR spectrum, in agreement with previous work on related complexes.^{8a,25} As these complexes can catalytically convert NADH to NAD^+ , it may be possible to disrupt this important redox couple in cells, which may have implications for cell metabolism, including lactate dehydrogenase-catalyzed lactate-pyruvate conversions,²⁶ enhancement of ROS levels,^{10,27} and reducing the concentration of one of the major electron donors in the electron transport chain.

Antiproliferative Activity. The antiproliferative activity of the 15 complexes covered a wide range, from 1 to $60 \mu\text{M}$ in A2780, 3.7 to $54.3 \mu\text{M}$ in HCT-116, 3.7 to $47 \mu\text{M}$ in MCF-7, and 2.1 to $89 \mu\text{M}$ in A549 cells, showing that the substituent on the chelating ligand has a significant effect on the antiproliferative activity of the complex. Complexes **2**, **8**, **13**, and **15** are all just as or more potent than the previously reported phenyl-extended Cp^{xPh} complex **17** ($\text{IC}_{50} = 2.14 \mu\text{M}$) toward A2780 cells, showing that the addition of functional groups to the 2-PhPy ligand can provide a strategy for increasing potency rather than functionalizing the Cp^{x} ligand. In contrast, complexes **3**, **4**, **7**, **9**, **10**, and **11** are less active toward A2780 cells than parent complex **16**. It is apparent that the presence of hydroxymethyl groups in complexes **9** and **10** decreases the antiproliferative activity. However, the presence of methyl groups enhances the activity, making them potentially interesting for further study. Methyl groups are inherently more likely to contribute to increased lipophilicity over hydroxymethyl groups, perhaps indicating that hydrophobicity is important for high potency.

The fluoro complexes **1** and **2**, in which the fluorine atom is situated on the phenyl ring, have promising activity of 2.7 and $4.4 \mu\text{M}$, respectively, whereas complexes **3** and **4**, in which the fluorine substituent is on the pyridyl ring, have IC_{50} values of $>50 \mu\text{M}$, demonstrating the contrasting biological activity of the structural isomers. This difference in activity for isomers is also observed for complexes **11** ($\text{IC}_{50} = 47.3 \mu\text{M}$) and **12** ($\text{IC}_{50} = 13.29 \mu\text{M}$), which contain hydroxyl groups on the phenyl and pyridyl ring, respectively, and for complexes **7** ($\text{IC}_{50} = 24.73 \mu\text{M}$) and **8** ($\text{IC}_{50} = 2.7 \mu\text{M}$), which bear a nitro group on the phenyl and pyridyl ring, respectively. Therefore, not only is the type of substituent important, but also where it is situated on

the chelating ligand. Previously, it has been demonstrated that inclusion of fluorine substituents on the chelating ligand of half-sandwich ruthenium and osmium complexes generally gave the most potent systems,²⁸ in contrast to the results obtained here. It has also been demonstrated that in half-sandwich iridium(III) complexes bearing picolinamide chelating ligands, the inclusion of a chlorine atom in the arene ring of the chelating ligand increases activity over the unfunctionalized complex.⁷ A further increase in activity was observed upon the introduction of a second chlorine atom depending on its position. However, the contrasting activities between structural isomers observed in this work are much greater than for the picolinamide complexes.

Relationship between Hydrophobicity, Iridium-Cellular Accumulation, and Potency. The complexes studied here are all neutral species in the presence of biologically relevant concentrations of sodium chloride. Hydrophobicity can promote interaction with the lipophilic cell membrane²⁹ and promote hydrophobic interactions with protein targets.³⁰ In general, the accumulation and potency of organometallic complexes in cells increases with an increase in their hydrophobicity.^{23c,31} The relative hydrophobicity of complexes **2**, **4**, **7**, **8**, and **11–14** (four pairs of structural isomers) was determined by RP-HPLC. As RP-HPLC relies on the relative interaction between the hydrophilic mobile phase and hydrophobic stationary phase, determination of the relative hydrophobicity of a series of complexes can be based on retention times (t_{R}). It was found that the nature of the substituent on the 2-PhPy ligand can dictate the hydrophobicity of the complex, with hydroxyl complexes **11** and **12** being the least lipophilic, while complexes **13** and **14**, bearing methyl groups, are the most. Intriguingly, complex **12** appeared to be much more hydrophobic than the corresponding structural isomer **11**, with retention times of 17.8 and 15.1 min, respectively (Figure S6). It is apparent that not only the type of substituent but also its position govern the hydrophobicity of the complex.

To examine if structural isomers accumulate in cells to a different extent, the cellular-iridium accumulation in A2780 cells of **2**, **4**, **7**, **8**, and **11–14** was determined at equipotent (IC_{50}) concentrations. For isomers **2/4** and **13/14** the levels of cellular-iridium accumulation are similar, with only small differences between them. Isomers **7/8** show no difference between their respective iridium accumulations. However, isomers **11/12** show contrasting levels of cellular-iridium accumulation, with **12** being accumulated 6 times more than **11** (10.2 vs $1.6 \text{ ng Ir} \times 10^6$ A2780 cells).

The hydrophobicity measurements were correlated with cellular-iridium accumulation in A2780 cells in order to investigate if hydrophobicity is important in their ability to enter cells (Figure 6a,b). There is a clear relationship between a higher hydrophobicity and an increase in cellular accumulation ($R^2 = 0.969$). Isomers **13** and **14** are the most hydrophobic complexes and accumulate in A2780 cells to the highest extent, while complex **11**, with the lowest hydrophobicity, showed the lowest accumulation. It was recently demonstrated that the structurally similar iridium(III) complex $[(\eta^5\text{-Cp}^*)\text{Ir}(7,8\text{-benzoquinoline})\text{Cl}]$ is transported into cells by both energy-independent passive diffusion and energy-dependent pathways.¹² Since an increase in hydrophobicity results in an increase in cellular accumulation, it is likely that passive diffusion plays at least a part in the mechanism of cellular accumulation for these complexes, making hydrophobicity an important design feature.

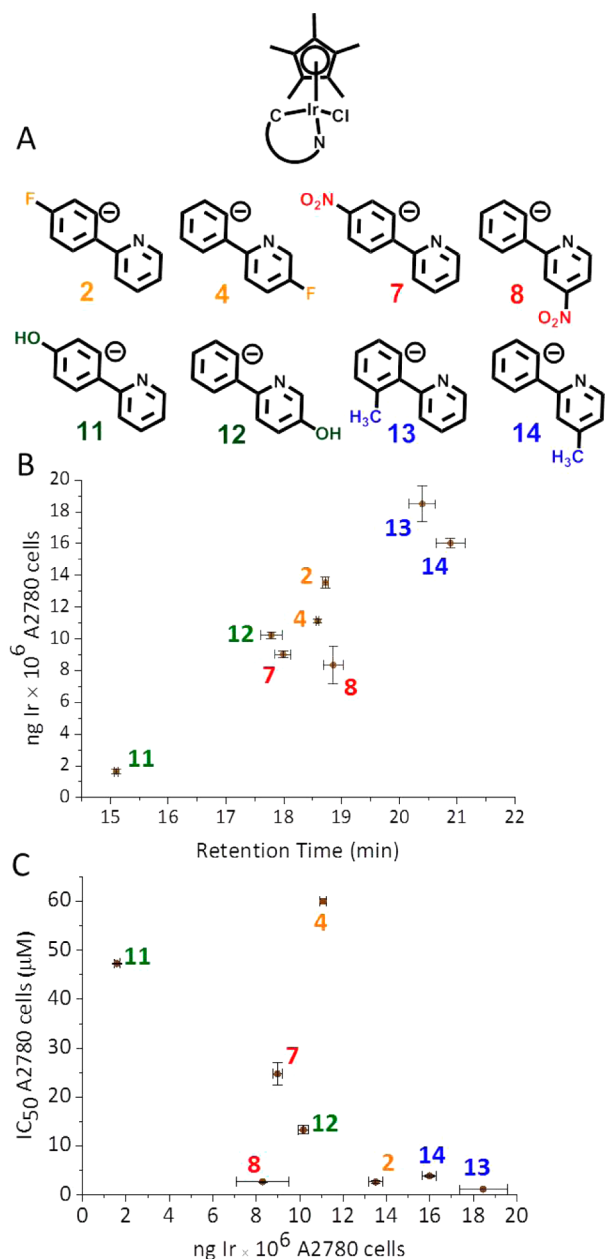


Figure 6. (a) Structures of complexes studied. (b) Plot of relative hydrophobicity, as indicated by retention times on RP-HPLC, against cellular accumulation of iridium at IC_{50} concentrations in A2780 cells, after exposure to complexes 2, 4, 7, 8, and 11–14, showing a correlation of hydrophobicity with cellular accumulation. (c) Comparison of cellular accumulation of iridium and antiproliferative activity of complexes 2, 4, 7, 8, and 11–14 in A2780 cells, showing that in general higher cellular accumulation results in more potent complexes.

The cellular-iridium accumulation was correlated with antiproliferative activity in A2780 cells, which shows that a pattern exists between enhanced accumulation and increase in potency (Figure 6c). Complex 11 exhibits the lowest cellular accumulation and second lowest potency ($1.58 \text{ ng Ir} \times 10^6$ cells, $47.3 \mu\text{M}$), and complex 13 exhibits the highest cellular accumulation and potency ($18.46 \text{ ng Ir} \times 10^6$ cells, $1.18 \mu\text{M}$). In the case of structural isomers 11 and 12, the difference in hydrophobicity of the complexes as a consequence of changing the position of the hydroxyl group on the 2-PhPy ligand results

in enhanced cellular accumulation for the more hydrophobic complex 12, which leads to a more potent complex. Interestingly, although 2 and 8 exhibit low IC_{50} values ($IC_{50} = 2.7 \mu\text{M}$), they show similar levels of cellular accumulation to their less potent structural isomers 4 ($IC_{50} > 60 \mu\text{M}$) and 7 ($IC_{50} = 24.73 \mu\text{M}$). As the iridium accumulation is performed at IC_{50} concentrations, this may indicate that the mechanism involved in the antiproliferative activity of complexes 2 and 8 is more efficient over their counterparts 4 and 7.

Cellular-Iridium Distribution of Isomers 2 and 4. The distribution of iridium in A2780 human ovarian cancer cells after exposure to structural isomers 2 and 4 follows the order of localization: cytosol > cell membrane and particulate > nucleus > cytoskeleton. Although both isomers followed the same trend, they do so to different extents. Complex 4 localizes in the cytosol to a greater extent than 2 (69.2% vs 51.4%), whereas 2 localizes in the cell membrane and particulate to a greater extent than 4 (28.4% vs 17.9%). The variations in localization preference arising from this small structural change may reflect the differences observed in antiproliferative activity.³² For example, if the biological target of these complexes is in the cell membrane and particulate fraction, then that may explain why isomer 2 is more active than 4. As the isomers exhibit dramatically different IC_{50} values yet both bind to guanine and accumulate in the nucleus to similar extents, DNA may not be the main biological target. It has also been shown that halogen-bonding interactions could be important in rational drug design;³³ therefore the position of fluorine within the ligand may influence the way the complexes interact with biomolecules, leading ultimately to variations in activity.

CONCLUSIONS

Interest in iridium(III) half-sandwich complexes as anticancer agents is increasing, with new complexes being reported and novel mechanisms of action being discovered.^{3a,7,10,11,34} In this work we have investigated the effects of electron-donating and electron-withdrawing substituents on C,N-chelating 2-PhPy ligands on the physicochemical and biological activity of their complexes.

DFT calculations show that the nature and position of the substituent have minimal effects on the electronic charge at the iridium center, Cp*, or chlorido ligands, but exert localized changes in the electrostatic potential surface and overall electron density of the chelating ligand. This finding provides potential for modulating the way the complexes interact with biological targets such as proteins and oligonucleotides.

All complexes hydrolyze rapidly at 310 K, but total suppression of aquation can be achieved with 4 mM NaCl, implying that under physiological conditions the complexes would exist as the neutral chlorido species. All complexes bind strongly to the nucleobase 9-EtG, even in the presence of 4 mM NaCl, indicating that DNA could be a target for these complexes. The observed catalytic oxidation of NADH might occur in cells and disturb the redox balance and is an interesting property of some iridium(III) half-sandwich anticancer complexes.^{8,35} The catalytic activity showed dependence on the substituent present on the 2-PhPy ligand, whereby hydroxyl substituents slightly enhanced the catalytic ability of the complex compared to fluorine. The oxidation of NADH appears to be mediated through the formation of Ir-H species, as detected by ¹H NMR spectroscopy.

The antiproliferative activity of the complexes is strongly dependent on the type of substituent and its position on the

chelating ligand, giving rise to contrasting activities between structural isomers despite exhibiting similar chemical behavior. The presence of substituents on the 2-PhPy ligand could in some cases generate complexes that are more potent than those bearing the extended Cp^{xph} ligand, thus providing an alternative strategy for increasing potency in these systems.

Further physicochemical analysis of these complexes showed that both the nature and position of substituent can determine their hydrophobicity and, consequently, affect the accumulation of Ir in A2780 cells. Correlation analysis showed that an increase in hydrophobicity results in an increase in cellular-Ir accumulation, which generally results in an increase in potency. Cellular-Ir distribution in A2780 cells of a pair of structural isomers that exhibit contrasting biological activity yet similar levels of Ir accumulation showed that the position of the substituent affects the extent of localization in cellular compartments, perhaps indicating that the less active isomer does not reach the biological target as efficiently as its active counterpart.

This study shows that small changes in the functionalization of the chelating ligands in half-sandwich iridium(III) complexes can have a profound effect on the biological activity of the complexes. Importantly, it also highlights that the inclusion of substituents in 2-PhPy ligands can provide complexes with enhanced potency without the use of extended cyclopentadienyl ligands, a strategy that could be beneficial for the development of this class of complexes.

EXPERIMENTAL SECTION

Materials. IrCl₃·nH₂O (99%) was purchased from Precious Metals Online (Australia). 1,2,3,4,5-Pentamethylcyclopentadiene, NaCl (>99.999%), tetrakis(triphenylphosphine)palladium (99%), phenylboronic acid, 6-bromo-3-pyridinecarboxaldehyde, 2-bromo-4-nitropyridine, 4-formylphenylboronic acid, 4-(hydroxymethyl)phenylboronic acid, 4-hydroxyphenylboronic acid, 2-bromo-4-hydroxymethylpyridine, 2-bromo-4-methylpyridine, 2-bromo-5-fluoropyridine (97%), *p*-tolylboronic acid (97%), 4-nitrophenylboronic acid (95%), 9-ethylguanine (≥98%), 9-methyladenine (97%), and β-nicotinamide adenine dinucleotide-reduced dipotassium salt (≥95%) were purchased from Sigma-Aldrich (UK). 2-Bromopyridine, 2-fluorophenylboronic acid, and 4-fluorophenylboronic acid were purchased from Fisher Scientific (UK), 2-bromo-5-hydroxypyridine and 2-bromo-5-methylpyridine were from VWR International Ltd. (UK), and 2-bromo-3-fluoropyridine was from Tokyo Chemical Industry Ltd. (UK). Solvents used for synthesis were of laboratory grade and used without further purification. Solvents for RP-HPLC (water and acetonitrile) were of HPLC grade with added trifluoroacetic acid (purchased from Sigma-Aldrich (UK)) for purity measurements. [(η⁵-Cp*)IrCl₂]₂ was synthesized according to a literature procedure.³⁶

Syntheses. *Synthesis of 2-(R'-phenyl)-R-pyridine Ligands.* The synthesis of ligands **L1–15** was performed using the following adapted literature procedure.¹³ Phenylboronic acid/derivatives (1.4 mol equiv) and 2-bromopyridine/derivatives (1 mol equiv) were dissolved in 1:1:1 (v/v) tetrahydrofuran/water/1 M aqueous sodium carbonate solution and stirred at ambient temperature under nitrogen for 1 h. Tetrakis(triphenylphosphine)palladium (2% cat) was added in one portion, and the reaction mixture was heated under reflux at 373 K for 24 h. The reaction mixture was cooled to ambient temperature and extracted with dichloromethane. The organic layer was washed with saturated sodium hydrogen carbonate solution and brine, then dried with magnesium sulfate, and concentrated to dryness, yielding the crude material. Purification by silica flash chromatography was performed using chloroform/ethyl acetate, yielding purified products. Characterization data are shown in the Supporting Information.

Synthesis of [(η⁵-Cp)Ir(2-(R'-phenyl)-R-pyridine)Cl] Complexes.* The synthesis of complexes **1–15** was performed using the following adapted literature procedure.^{4b} 2-(R'-phenyl)-R-pyridine (2 molar equiv) was dissolved in anhydrous dichloromethane, sodium acetate (4 molar equiv) was added in one portion, and the mixture was stirred at ambient temperature under nitrogen for 30 min. [(η⁵-Cp*)IrCl₂]₂ (1 molar equiv) was added in one portion, and the reaction mixture stirred at ambient temperature for 18 h. The mixture was filtered through Celite under suction, and the filtrate was concentrated to dryness on a rotary evaporator. The crude product was recrystallized from chloroform/hexane at 273 K to yield purified complexes. Characterization data are shown in the Supporting Information.

Methods and Instrumentation. *X-ray Crystallography.* Diffraction data for complexes **1** and **2** were obtained on an Oxford Diffraction Gemini four-circle system with a Ruby CCD area detector using Mo Kα radiation. Absorption corrections were applied using ABSPACK.³⁷ The crystals were mounted in oil and held at 100 K with the Oxford Cryosystem Cobra. The structures were solved by direct methods using SHELXS (TREF)³⁸ with additional light atoms found by Fourier methods. Complexes were refined against F² using SHELXL.³⁹

X-ray crystallographic data for complexes **1** and **2** have been deposited in the Cambridge Crystallographic Data Centre under the accession numbers CCDC 1043863 and 1043864, respectively.

NMR Spectroscopy. ¹H NMR spectra were obtained in 5 mm NMR tubes at 298 K (unless stated otherwise) on either Bruker DPX-300, Bruker DPX-400, or AV III 600 NMR spectrometers. ¹H NMR chemical shifts were internally referenced to (CHD₂)(CD₃)SO (2.50 ppm) for DMSO-*d*₆, CHCl₃ (7.26 ppm) for chloroform-*d*₁, (CHD₂)-(CD₃)CO (2.05 ppm) for acetone-*d*₆, and 1,4-dioxane (3.75 ppm) for aqueous solutions. ¹³C NMR data were obtained in 5 mm NMR tubes at 298 K on a Bruker AV III-500 HD NMR spectrometer. ¹³C NMR chemical shifts were internally referenced to CDCl₃ (77.16 ppm) for chloroform-*d*₁, (CD₃)₂SO (39.52 ppm) for DMSO-*d*₆, and (CD₃)₂CO (29.84 ppm) for acetone-*d*₆. The data were processed using TOPSPIN (version 2.1 Bruker UK Ltd.).

Mass Spectrometry. ESI-MS were obtained on a Bruker Esquire 2000 ion trap spectrometer. Samples were prepared in either MeOH or CH₃CN. The mass spectra were recorded with a scan range of either *m/z* 50–500 or *m/z* 400–100 for positive ions. Data were processed using Data Analysis 3.3 (Bruker Daltonics).

Elemental Analysis. CHN elemental analyses were carried out on a CE-440 elemental analyser by Exeter Analytical (UK) Ltd.

pH Measurements. pH and pH* (pH meter reading without correction for the effect of deuterium on the glass electrode) were measured at ambient temperature using a miniLab IQ125 pH meter, pH sensor, and referenced to KCl gel.

HPLC. Purity measurements by HPLC were performed using the Agilent 1200 system with a VDW and 100 μL loop. The column used was an Agilent Zorbax Eclipse Plus C18, 250 × 4.6 mm with a 5 μm pore size. Mobile phase used was H₂O 0.1% TFA/MeCN 0.1% TFA at gradients of *t* = 0 min 10% B, *t* = 30 min 80% B, *t* = 40 min 80% B, *t* = 41 min 10% B, and *t* = 55 min 10% B over a 55 min period. Flow rate was 1 mL min⁻¹, and the detection wavelength was set at 254 nm with the reference wavelength at either 360 or 510 nm. Sample injections were half the loop volume (50 μL) with needle washes of MeOH and H₂O between injections. It was assumed that all species in a sample have the same extinction coefficient at 254 nm. All peaks were manually integrated to gain the percentage area. Samples were dissolved in 2.7% DMSO/97.3% H₂O at ca. 100 μM.

Computation. Calculations were performed using the Gaussian 03 package.¹⁵ Geometry optimization calculations were performed in the gas phase with the hybrid functional PBE1PBE.^{14a} The LanL2DZ basis set and effective core potential^{14b} were used for the Ir atom, and the 6-31+G** basis set was used for all other atoms.^{14c} The nature of all stationary points was confirmed by performing a normal-mode analysis. Electrostatic potential surfaces for complexes **2**, **4**, **7**, **8**, and **11–13** are shown both in space (with positive and negative regions in blue and red, respectively) and mapped on electron density (isovalue

0.04) of the molecules. The electrostatic potential is represented with a color scale ranging from red (-0.040 au) to blue ($+0.250$ au).

Inductively Coupled Plasma–Optical Emission Spectrometry (ICP-OES). ICP-OES analyses were carried out on a PerkinElmer Optima 5300 DV series ICP-OES instrument. The water used for ICP-OES analysis was doubly deionized (DDW) using a Millipore Milli-Q water purification system and a USF Elga UHQ water deionizer. The iridium Specupure plasma standard (Alfa Asar, 1000 pm in 10% HCl) was diluted with 2.5% HNO₃ DDW to freshly prepare calibrants at concentrations of 1000, 800, 600, 400, 200, and 100 ppb, which were spiked with NaCl to match the salt content of the samples being analyzed.

Inductively Coupled Plasma–Mass Spectrometry (ICP-MS). ICP-MS analyses were carried out on an Agilent Technologies 7500 series ICP-MS instrument. The water used for ICP-MS analysis was doubly deionized using a Millipore Milli-Q water purification system and a USF Elga UHQ water deionizer. The iridium Specupure plasma standard (Alfa Asar, 1000 pm in 10% HCl) was diluted with 2.5% HNO₃ DDW to prepare calibrants freshly at concentrations of 100, 80, 60, 40, 20, 5, 1, 0.8, and 0.5 ppb. The ICP-MS instrument was set to detect ¹⁹³Ir using no gas mode.

Hydrolysis Studies. The aquation of complexes (*ca.* 500 μ M) was monitored by ¹H NMR spectroscopy over 24 h in 26.7% MeOD/73.3% D₂O at 310 K using a Bruker AV III 600 NMR spectrometer. All spectra were internally referenced to 1,4-dioxane (3.75 ppm), and water suppression was performed using Shaka techniques.⁴⁰ NaCl was added to aid assignment of species to either the Ir-OD₂ or Ir-Cl adducts. Percentages of each adduct were calculated based on ¹H NMR peak integrations.

Reactions with DNA Nucleobases. Interactions of complexes (*ca.* 500 μ M) with 9-ethylguanine and 9-methyladenine (*ca.* 500 μ M) were studied by ¹H NMR spectroscopy for periods of 15 min and 24 h after addition of the nucleobase(s) in 26.7% MeOD/73.3% D₂O at 310 K using a Bruker AV III 600 NMR spectrometer.

Hydrophobicity Determinations. Relative hydrophobicity measurements by HPLC were performed using the Agilent 1200 system with a VDW and 100 μ L loop. The column used was an Agilent Zorbax Eclipse Plus C18, 150 \times 4.6 mm with a 5 μ m pore size. Mobile phase used was H₂O 50 mM NaCl/H₂O/MeCN 1:1 50 mM NaCl at gradients of $t = 0$ –20% B, $t = 15$ min 100% B, $t = 40$ min 100% B, $t = 42$ min 20% B, and $t = 57$ min 20% B over a 57 min period. Flow rate was 1 mL min⁻¹, and the detection wavelength was set at 254 nm with the reference wavelength at 360 nm. Sample injections were half the loop volume (50 μ L) with needle washes of H₂O between injections. Samples were dissolved in 10% MeOH/90% H₂O in 50 mM NaCl at *ca.* 100 μ M. Reported retention times (t_R) and standard deviations (SD) are from duplicates of triplicate measurements.

Catalytic Oxidation of NADH to NAD⁺. Complexes were evaluated for the catalytic oxidation of NADH to NAD⁺ by UV–visible spectroscopy over a 24 h period in 0.5% MeOH/99.5% H₂O at 310 K in 5 mM Na₂HPO₄/NaH₂PO₄ buffer, pH 7.5. The complex concentration remained fixed at 2.5 μ M with NADH concentrations of 69, 103, 127, and 146 μ M. The conversion of NADH to NAD⁺ was followed by absorption at 339 nm ($\epsilon_{\text{NADH}} = 6220 \text{ cm}^{-1} \text{ M}^{-1}$) to allow evaluation of kinetic data.

The reaction between complex 2 (250 μ M) and NADH (750 μ M) in 50% MeOD/50% H₂O at 310 K, pH* 7.4, was monitored by ¹H NMR spectroscopy.

Cell Experiments. The cell lines used in this work, A2780 human ovarian carcinoma, A549 human Caucasian lung carcinoma, HCT116 human colon carcinoma, and MCF7 human Caucasian breast carcinoma, were obtained from the European Collection of Cell Cultures (ECACC). A2780 ovarian cells were grown in Roswell Park Memorial Institute medium (RPMI-1640), A549 and MCF7 in Dulbecco's modified Eagle medium (DMEM), and HCT116 in McCoy's modified 5A medium. All media were supplemented with 10% v/v fetal calf serum, 1% v/v 2 mM glutamine, and 1% v/v penicillin/streptomycin.

All cells were grown in 75 cm² culture flasks as adherent monolayers, and they were split two to three times a week when

around 80–90% confluence was reached, using 0.25% v/v trypsin for A2780 and 0.25% v/v trypsin/EDTA for all other cell lines.

In Vitro Growth Inhibition Assay. Briefly, 96-well plates were used to seed 5000 cells per well; they were left to preincubate in drug-free media at 310 K for 48 h before adding various concentrations of the compounds to be tested. Stock solutions of the Ir complexes were first prepared in 5% v/v DMSO and a mixture of 0.9% w/v saline and medium (1:1) following serial dilutions in the corresponding cell culture medium. A drug exposure period of 24 h was allowed. After this, the supernatant were removed by suction, and each well was washed with PBS. A further 72 h was allowed for the cells to recover in drug-free medium at 310 K. The SRB assay was used to determine cell viability. This assay, first developed by Skeham et al. in 1990, is based on the ability of the sulforhodamine B to bind electrostatically to basic amino acid residues of proteins from fixed cells. Absorbance measurements of solubilized dye allow the determination of the amount of viable treated cells against an untreated control. These measurements were carried out using a BioRad iMark microplate reader with a 470 nm filter. IC₅₀ values, as the concentration that causes 50% of inhibition of cell growth, were determined as duplicates of triplicates in two independent sets of experiments, and their standard deviations calculated.

Metal Accumulation in Cancer Cells. Metal accumulation studies for complexes 2, 4, 7, 8, and 11–14 were conducted on the A2780 ovarian carcinoma cell line. Briefly, 1.5×10^6 cells were seeded on a six-well plate, after 24 h of preincubation time in drug-free medium, at 310 K in a 5% CO₂ humidified atmosphere; the test complexes were added to give final concentrations equal to IC₅₀ and then allowed a further 24 h of drug exposure under similar conditions. After this time, cells were treated with trypsin and counted, and cell pellets were collected. Each pellet was digested overnight in concentrated nitric acid (73%) at 353 K; the resulting solutions were diluted to 5% v/v HNO₃ using doubly deionized water, and the amount of iridium taken up by the cells was determined by ICP-MS, using an Agilent Technologies 7500 series instrument. The solvent used for all ICP-MS experiments was DDW with 5% v/v HNO₃. Metal standards (Ir) were freshly prepared before each experiment. The concentrations used for the calibration curve were 0, 0.5, 0.8, 1, 5, 20, 40, 60, 80, and 100 ppb. The isotope detected was ¹⁹³Ir; readings were made in duplicate (no-gas mode). These experiments did not include any cell recovery time in drug-free media. They were all carried out in triplicate in two sets of independent experiments, and the standard deviations were calculated.

Metal Distribution in A2780 Cells for Complexes 2 and 4. Cell pellets were obtained as described above and were fractionated using the FractionPREP kit from BioVision according to the supplier's instructions. Each sample was digested overnight in concentrated nitric acid (73%), and the amount of Ir taken up by the cells was determined by ICP-MS. These experiments were all carried out in triplicate, and the standard deviations were calculated. Statistical significance between results was established from the Student's *t* test, where ** = $p < 0.01$.

■ ASSOCIATED CONTENT

📄 Supporting Information

Selected X-ray crystallographic data for complexes 1 and 2 (Table S1), calculated bond lengths and HOMO and LUMO orbital diagrams and energies (Tables S2 and S3), intermolecular stacking features (Figure S1), aqueous chemistry and nucleobase binding (Figures S2 and S3), NADH reaction kinetics and hydride formation (Figures S4 and S5), relative hydrophobicity HPLC traces (Figure S6), and Cartesian coordinates determined by DFT calculations are available in the SI. Cartesian coordinates for DFT calculations are also supplied in .xyz format. These materials are available free of charge via the Internet at <http://pubs.acs.org>. X-ray crystallographic data in CIF format are available from the Cambridge Crystallographic Data Centre (<http://www.ccdc.cam.ac.uk>).

AUTHOR INFORMATION

Corresponding Author

*E-mail: P.J.Sadler@warwick.ac.uk

Notes

The authors declare no competing financial interest.

ACKNOWLEDGMENTS

We thank the ERC (grant no. 247450), EPSRC (grant no. EP/F034210/1), and Science City (AWM/ERDF) for support and members of EU COST Action CM1105 for stimulating discussions. We thank Prof. Rob Deeth for advice on DFT calculations, Dr. Ivan Prokes for acquiring ^{13}C NMR data, and the Dalton division of the RSC for a travel grant for A.J.M. to present this research at AsBIC7.

DEDICATION

We dedicate this article to Mike Lappert, who inspired organometallic chemists over many years.

REFERENCES

- (1) (a) Garbutcheon-Singh, K. B. G. M. P.; Harper, B. W.; Krause-Heuer, A. M.; Manohar, M.; Orkey, N.; Aldrich-Wright, J. R. *Curr. Top. Med. Chem.* **2011**, *11*, 521–542. (b) Sava, G.; Bergamo, A.; Dyson, P. J. *Dalton Trans.* **2011**, *40*, 9069–9075. (c) Hartinger, C. G.; Metzler-Nolte, N.; Dyson, P. J. *Organometallics* **2012**, *31*, 5677–5685. (d) Ma, D.-L.; Chan, D. S.-H.; Leung, C.-H. *Acc. Chem. Res.* **2014**, *47*, 3614–3631. (e) Chow, M. J.; Licon, C.; Yuan Qiang Wong, D.; Pastorin, G.; Gaidon, C.; Ang, W. H. *J. Med. Chem.* **2014**, *57*, 6043–6059. (f) Ma, D.-L.; Liu, L.-J.; Leung, K.-H.; Chen, Y.-T.; Zhong, H.-J.; Chan, D. S.-H.; Wang, H.-M. D.; Leung, C.-H. *Angew. Chem., Int. Ed.* **2014**, *53*, 9178–9182.
- (2) (a) Tripathy, S. K.; De, U.; Dehury, N.; Pal, S.; Kim, H. S.; Patra, S. *Dalton Trans.* **2014**, *43*, 14546–14549. (b) Romero-Canelón, I.; Salassa, L.; Sadler, P. J. *J. Med. Chem.* **2013**, *56*, 1291–1300. (c) Furrer, M. A.; Garci, A.; Denoyelle-Di-Muro, E.; Trouillas, P.; Giannini, F.; Furrer, J.; Clavel, C. M.; Dyson, P. J.; Süß-Fink, G.; Therrien, B. *Chem.—Eur. J.* **2013**, *19*, 3198–3203.
- (3) (a) Novohradsky, V.; Zerzankova, L.; Stepankova, J.; Kisova, A.; Kosthunova, H.; Liu, Z.; Sadler, P. J.; Kasparkova, J.; Brabec, V. *Metallomics* **2014**, *6*, 1491–1501. (b) Ludwig, G.; Randelović, I.; Maksimović-Ivanić, D.; Mijatović, S.; Bulatović, M. Z.; Miljković, D.; Korb, M.; Lang, H.; Steinborn, D.; Kaluđerović, G. N. *ChemMedChem* **2014**, *9*, 1586–1593. (c) Payne, R.; Govender, P.; Therrien, B.; Clavel, C. M.; Dyson, P. J.; Smith, G. S. *J. Organomet. Chem.* **2013**, *729*, 20–27. (d) Hearn, J. M.; Romero-Canelón, I.; Qamar, B.; Liu, Z.; Hands-Portman, I.; Sadler, P. J. *ACS Chem. Biol.* **2013**, *8*, 1335–1343. (e) Lucas, S. J.; Lord, R. M.; Wilson, R. L.; Phillips, R. M.; Sridharan, V.; McGowan, P. C. *Dalton Trans.* **2012**, *41*, 13800–13802. (f) Gupta, G.; Kumar, J.; Garci, A.; Nagesh, N.; Therrien, B. *Molecules* **2014**, *19*, 6031–6046. (g) Li, Y.; Tan, C.-P.; Zhang, W.; He, L.; Ji, L.-N.; Mao, Z.-W. *Biomaterials* **2015**, *39*, 95–104. (h) Ruiz, J.; Vicente, C.; de Haro, C.; Bautista, D. *Inorg. Chem.* **2013**, *52*, 974–982. (i) Leung, C.-H.; Liu, L.-J.; Lu, L.; He, B.; Kwong, D. W. J.; Wong, C.-Y.; Ma, D.-L. *Chem. Commun.* **2015**, *51*, 3973–3976.
- (4) (a) Liu, Z.; Habtemariam, A.; Pizarro, A. M.; Fletcher, S. A.; Kisova, A.; Vrana, O.; Salassa, L.; Bruijninx, P. C. A.; Clarkson, G. J.; Brabec, V.; Sadler, P. J. *J. Med. Chem.* **2011**, *54*, 3011–3026. (b) Liu, Z.; Habtemariam, A.; Pizarro, A. M.; Clarkson, G. J.; Sadler, P. J. *Organometallics* **2011**, *30*, 4702–4710.
- (5) Liu, Z.; Salassa, L.; Habtemariam, A.; Pizarro, A. M.; Clarkson, G. J.; Sadler, P. J. *Inorg. Chem.* **2011**, *50*, 5777–5783.
- (6) Wirth, S.; Rohbogner, C.; Cieslak, M.; Kazmierczak-Baranska, J.; Donevski, S.; Nawrot, B.; Lorenz, I.-P. *J. Biol. Inorg. Chem.* **2010**, *15*, 429–440.
- (7) Almodares, Z.; Lucas, S. J.; Crossley, B. D.; Basri, A. M.; Pask, C. M.; Hebden, A. J.; Phillips, R. M.; McGowan, P. C. *Inorg. Chem.* **2014**, *53*, 727–736.
- (8) (a) Liu, Z.; Deeth, R. J.; Butler, J. S.; Habtemariam, A.; Newton, M. E.; Sadler, P. J. *Angew. Chem., Int. Ed.* **2013**, *52*, 4194–4197. (b) Betanzos-Lara, S.; Liu, Z.; Habtemariam, A.; Pizarro, A. M.; Qamar, B.; Sadler, P. J. *Angew. Chem., Int. Ed.* **2012**, *51*, 3897–3900. (9) Romero-Canelón, I.; Sadler, P. J. *Inorg. Chem.* **2013**, *52*, 12276–12291.
- (10) Liu, Z.; Romero-Canelón, I.; Qamar, B.; Hearn, J. M.; Habtemariam, A.; Barry, N. P. E.; Pizarro, A. M.; Clarkson, G. J.; Sadler, P. J. *Angew. Chem., Int. Ed.* **2014**, *53*, 3941–3946.
- (11) (a) Ruiz, J.; Rodriguez, V.; Cutillas, N.; Samper, K. G.; Capdevila, M.; Palacios, O.; Espinosa, A. *Dalton Trans.* **2012**, *41*, 12847–12856. (b) Geldmacher, Y.; Splith, K.; Kitanovic, I.; Alborzina, H.; Can, S.; Rubbiani, R.; Nazif, M.; Wefelmeier, P.; Prokop, A.; Ott, I.; Wöfl, S.; Neundorff, I.; Sheldrick, W. J. *Biol. Inorg. Chem.* **2012**, *17*, 631–646.
- (12) Novohradsky, V.; Liu, Z.; Vojtiskova, M.; Sadler, P. J.; Brabec, V.; Kasparkova, J. *Metallomics* **2014**, *6*, 682–690.
- (13) Steunenberg, P.; Ruggi, A.; van den Berg, N. S.; Buckle, T.; Kuil, J.; van Leeuwen, F. W. B.; Velders, A. H. *Inorg. Chem.* **2012**, *51*, 2105–2114.
- (14) (a) Adamo, C.; Barone, V. *J. Chem. Phys.* **1999**, *110*, 6158–6170. (b) Hay, P. J.; Wadt, W. R. *J. Chem. Phys.* **1985**, *82*, 270–283. (c) McLean, A. D.; Chandler, G. S. *J. Chem. Phys.* **1980**, *72*, 5639–5648.
- (15) Frisch, M. J.; Trucks, G. W.; Schlegel, H. B.; Scuseria, G. E.; Robb, M. A.; C, J. R.; Montgomery, J. A., Jr.; Vreven, T.; Kudin, K. N.; B, J. C.; Millam, J. M.; Iyengar, S. S.; Tomasi, J.; Barone, V.; M, B.; Cossi, M.; Scalmani, G.; Rega, N.; Petersson, G. A.; N, H.; Hada, M.; Ehara, M.; Toyota, K.; Fukuda, R.; H, J.; Ishida, M.; Nakajima, T.; Honda, Y.; Kitao, O.; Nakai, H.; K, M.; Li, X.; Knox, J. E.; Hratchian, H. P.; Cross, J. B.; Bakken, V.; A, C.; Jaramillo, J.; Gomperts, R.; Stratmann, R. E.; Yazyev, O.; A, A. J.; Cammi, R.; Pomelli, C.; Ochterski, J. W.; Ayala, P. Y.; M, K.; Voth, G. A.; Salvador, P.; Dannenberg, J. J.; Zakrzewski, V. G.; D, S.; Daniels, A. D.; Strain, M. C.; Farkas, O.; M, D. K.; Rabuck, A. D.; Raghavachari, K.; Foresman, J. B.; O, J. V.; Cui, Q.; Baboul, A. G.; Clifford, S.; Cioslowski, J.; S, B. B.; Liu, G.; Liashenko, A.; Piskorz, P.; Komaromi, I.; M, R. L.; Fox, D. J.; Keith, T.; Al-Laham, M. A.; Peng, C. Y.; N, A.; Challacombe, M.; Gill, P. M. W.; Johnson, B.; C, W.; Wong, M. W.; Gonzalez, C.; Pople, J. A. *Gaussian 03*, Revision D.02; Gaussian, Inc.: Wallingford, CT, 2004.
- (16) Lichter, R. L.; Wasylishen, R. E. *J. Am. Chem. Soc.* **1975**, *97*, 1808–1813.
- (17) (a) Park-Gehrke, L. S.; Freudenthal, J.; Kaminsky, W.; DiPasquale, A. G.; Mayer, J. M. *Dalton Trans.* **2009**, 1972–1983. (b) Li, L.; Brennessel, W. W.; Jones, W. D. *Organometallics* **2009**, *28*, 3492–3500.
- (18) Burgoyne, N. J.; Jackson, R. M. *Bioinformatics* **2006**, *22*, 1335–1342.
- (19) Dadci, L.; Elias, H.; Frey, U.; Hoernig, A.; Koelle, U.; Merbach, A. E.; Paulus, H.; Schneider, J. S. *Inorg. Chem.* **1995**, *34*, 306–315.
- (20) Helm, L.; Merbach, A. E. *Coord. Chem. Rev.* **1999**, *187*, 151–181.
- (21) (a) Takahara, P. M.; Rosenzweig, A. C.; Frederick, C. A.; Lippard, S. J. *Nature* **1995**, *377*, 649–652. (b) Pizarro, A. M.; Sadler, P. J. *Biochimie* **2009**, *91*, 1198–1211. (c) Liu, H.-K.; Berners-Price, S. J.; Wang, F.; Parkinson, J. A.; Xu, J.; Bella, J.; Sadler, P. J. *Angew. Chem.* **2006**, *118*, 8333–8336.
- (22) Pullman, B.; Pullman, A. *Biochim. Biophys. Acta* **1959**, *36*, 343–350.
- (23) (a) Fu, Y.; Romero, M. J.; Habtemariam, A.; Snowden, M. E.; Song, L.; Clarkson, G. J.; Qamar, B.; Pizarro, A. M.; Unwin, P. R.; Sadler, P. J. *Chem. Sci.* **2012**, *3*, 2485–2494. (b) Betanzos-Lara, S.; Salassa, L.; Habtemariam, A.; Novakova, O.; Pizarro, A. M.; Clarkson, G. J.; Liskova, B.; Brabec, V.; Sadler, P. J. *Organometallics* **2012**, *31*, 3466–3479. (c) Ruiz, J.; Rodríguez, V.; Cutillas, N.; Espinosa, A.; Hannon, M. J. *Inorg. Chem.* **2011**, *50*, 9164–9171.

- (24) Fujita, K.-i.; Yoshida, T.; Imori, Y.; Yamaguchi, R. *Org. Lett.* **2011**, *13*, 2278–2281.
- (25) Maenaka, Y.; Suenobu, T.; Fukuzumi, S. *J. Am. Chem. Soc.* **2011**, *134*, 367–374.
- (26) Ying, W. *Antioxid. Redox Signaling* **2007**, *10*, 179–206.
- (27) Dougan, S. J.; Habtemariam, A.; McHale, S. E.; Parsons, S.; Sadler, P. J. *Proc. Nat. Acad. Sci. U.S.A.* **2008**, *105*, 11628–11633.
- (28) Meier, S. M.; Hanif, M.; Adhireksan, Z.; Pichler, V.; Novak, M.; Jirkovsky, E.; Jakupec, M. A.; Arion, V. B.; Davey, C. A.; Keppler, B. K.; Hartinger, C. G. *Chem. Sci.* **2013**, *4*, 1837–1846.
- (29) Kerns, E. H.; Di, L. *Drug-like Properties: Concepts, Structure Design and Methods from ADME to Toxicity Optimization*, 1st ed.; Elsevier Academic Press: CA, 2008.
- (30) Hansch, C.; Maloney, P. P.; Fujita, T.; Muir, R. M. *Nature* **1962**, *194*, 178–180.
- (31) (a) Mendoza-Ferri, M.-G.; Hartinger, C. G.; Eichinger, R. E.; Stolyarova, N.; Severin, K.; Jakupec, M. A.; Nazarov, A. A.; Keppler, B. K. *Organometallics* **2008**, *27*, 2405–2407. (b) van Rijt, S. H.; Mukherjee, A.; Pizarro, A. M.; Sadler, P. J. *J. Med. Chem.* **2009**, *53*, 840–849. (c) Hanif, M.; Nazarov, A. A.; Hartinger, C. G.; Kandioller, W.; Jakupec, M. A.; Arion, V. B.; Dyson, P. J.; Keppler, B. K. *Dalton Trans.* **2010**, *39*, 7345–7352.
- (32) (a) Capobianco, J. O.; Zakula, D.; Frost, D. J.; Goldman, R. C.; Li, L.; Klein, L. L.; Lartey, P. A. *Antimicrob. Agents Chemother.* **1998**, *42*, 389–393. (b) Shaul, P.; Frenkel, M.; Goldstein, E. B.; Mittelman, L.; Grunwald, A.; Ebenstein, Y.; Tsarfaty, I.; Fridman, M. *ACS Med. Chem. Lett.* **2013**, *4*, 323–328.
- (33) Lu, Y.; Shi, T.; Wang, Y.; Yang, H.; Yan, X.; Luo, X.; Jiang, H.; Zhu, W. *J. Med. Chem.* **2009**, *52*, 2854–2862.
- (34) Liu, Z.; Romero-Canelón, I.; Habtemariam, A.; Clarkson, G. J.; Sadler, P. J. *Organometallics* **2014**, *33*, 5324–5333.
- (35) (a) Liu, Z.; Sadler, P. J. *Inorg. Chem. Front.* **2014**, *1*, 668–672. (b) Liu, Z.; Sadler, P. J. *Acc. Chem. Res.* **2014**, *47*, 1174–1185.
- (36) Tönnemann, J.; Risse, J.; Grote, Z.; Scopelliti, R.; Severin, K. *Eur. J. Inorg. Chem.* **2013**, *2013*, 4558–4562.
- (37) *CrysAlis PRO*; Oxford Diffraction Ltd.: Abington, Oxfordshire, U.K., 2007.
- (38) Sheldrick, G. *Acta Crystallogr., Sect. A: Found. Crystallogr.* **1990**, *46*, 467–473.
- (39) Sheldrick, G. *SHELXL-97*; Univeristy of Göttingen: Göttingen, Germany, 1997.
- (40) Hwang, T. L.; Shaka, A. J. *J. Magn. Reson.* **1995**, *112*, 275–279.